Remote Sensing of Environment 204 (2018) 401–411

Contents lists available at ScienceDirect

Remote Sensing of Environment

journal homepage: www.elsevier.com/locate/rse

LST retrieval algorithm adapted to the Amazon evergreen forests using MODIS data

José Gomis-Cebolla, Juan Carlos Jimenez*, José Antonio Sobrino

Global Change Unit, Image Processing Laboratory, University of Valencia, Paterna, Valencia 46010, Spain

A B S T R A C T

Amazonian tropical forests play a significant role in global water, carbon and energy cycles. Considering the importance of this biome and climate change projections, the monitoring of vegetation status of these rainforests becomes of significant importance. In this context vegetation temperature is presented as a key variable linked with plant physiology. In particular some studies showed the relationship between this variable and the CO_2 absorption capacity and biomass loss of these tropical forests proving the potential use of vegetation temperature in the monitoring of the vegetation status. Nevertheless, the use of thermal remote sensing data over tropical forests still has some limitations being of special importance the atmospheric correction under very humid conditions and the possible high occurrence of cloudy pixels. In order to mitigate these limitations over the Amazon region, we present in this paper a new processing methodology to derive a LST product from Moderate Resolution Imaging Spectroradiometer (MODIS) data. The LST product was generated using a tuned split-window equation and cloud information derived from the Multi-Angle Implementation of Atmospheric Correction (MAIAC) algorithm. This LST product was validated using simulated and in situ data, and inter-compared to the MODIS LST standard product (MOD11). Validation analysis shows that the new LST product reduces the RMSE by 0.6 to 1 K when compared to the MODIS standard LST product, mainly because of a reduction of the bias. We also show a preliminary intercomparison between MODIS and Visible Infrared Imaging Radiometer Suite (VIIRS) LST spatial patterns to illustrate the feasibility of VIIRS to extend forward the MODIS LST temporal series.

1. Introduction

Amazon rainforests, including more than the 50% of the world's tropical rainforests (Malhi et al., 2008) and accounting for approximately 25% of world's terrestrial species (Dirzo and Raven, 2003) play a crucial role in the global water cycle (Werth and Avissar, 2002) and global carbon cycle (Malhi et al., 2008). Additionally this region has attracted the attention of the scientific community due to the effects that minor modifications of this ecosystem could cause on local, regional and global climate (Gedney and Valdes, 2000; Werth and Avissar, 2002; Jiménez-Muñoz et al., 2016).

Thus considering the importance of this biome and the current global warming scenario an accurate monitoring of the vegetation changes is of special importance. In this context, satellite remote sensing provides the only viable means to observe the Amazon in a spatially comprehensive and temporally frequent fashion. Particularly, the Moderate Resolution Imaging Spectroradiometer (MODIS) onboard the NASA Terra and Aqua Earth Observation polar orbiting system satellites providing multiple day products is among today's major tools for the climate monitoring of this region (Hilker et al., 2015; Jiménez-Muñoz et al., 2013). In the recent years the majority of the studies have focused on the use of vegetation indexes derived using visible (VIS) and near-infrared (NIR) spectral information for the status monitoring of the region. However, this approach has some important limitations, mainly due to imperfect cloud masking and atmospheric correction, as well as difficulties that arise when removing directional effects (Hilker et al., 2012).

On the contrary less attention has been paid to the use of thermal infrared spectral range (TIR) information, with only the studies of Toomey et al. (2011) and Jiménez-Muñoz et al. (2013, 2015a,b) were the major contributions. In their studies a significant and sustained warming was revealed from an analysis of land surface temperatures anomalies using MODIS LST products (MOD11) and climatic data. This helps to prove the valuable information that could be derived from monitoring LST anomalies for the region. Additionally, vegetation temperature is a key variable linked with plant physiology. Particularly

* Corresponding author.
E-mail address: jcjm@uv.es (J.C. Jimenez).

http://dx.doi.org/10.1016/j.rse.2017.10.015
Received 7 June 2017; Received in revised form 26 September 2017; Accepted 13 October 2017
Available online 06 November 2017
0034-4257/ © 2017 Elsevier Inc. All rights reserved.

some studies have investigated the relationship between this variable and the CO_2 absorption capacity, showing that an increase in temperature could result in a negative impact on tropical forest CO_2 uptake and productivity (Doughty and Goulden, 2008; Clark et al., 2003). Also, anomalous high values have been proved to be more important than precipitation deficits in causing losses of biomass during drought periods (Galbraith et al., 2010). However the assessment of the Amazonian tropical forests status in the TIR spectral region shares the same limitations as its VIS/NIR counterpart being the most important the possible temperature alterations introduced by cloud-contamination. In particular, for the MODIS sensor, recent studies showed a land cover bias in the MODIS cloud mask (Leinenkugel et al., 2013) and how it could interfere in the derived MODIS land products, such as the LST product (Wilson et al., 2014). Additionally, cloud contamination for the MODIS LST products (MOD11) were reported in the literature, although for different biomes (Østby et al., 2014; Williamson et al., 2013, Westermann et al., 2012). For the Amazon region recent efforts have been done in order to quantify this effect and provide accurate cloud filtered LST data (Jiménez-Muñoz et al., 2015b; Gomis-Cebolla et al., 2016).

This paper is aimed at introducing a daytime product which could help to refine the LST estimations over this region, as well as to report the differences observed between this new product and the existing MODIS standard daytime LST product. The product presented in this paper benefits for the development of specific algorithm coefficients and the introduction of the cloud mask derived from the MAIAC algorithm. This cloud mask has shown promising results in comparison with MODIS collection 5 cloud mask (Lyapustin et al., 2008) and with a good performance in comparison with MODIS cloud mask over tropical ecosystems (Hilker et al., 2012).

The paper is organized as follows: In Section 2 the satellite data employed together with a description of the validation site is presented. In Section 3 the LST algorithm is presented and evaluated. In Section 4 an overview of the MAIAC cloud mask performance in comparison with the MODIS cloud-screening methodology used in MODIS LST products (MOD11) is presented. In Section 5, the results from LST products presented here and the MODIS LST products (MOD11) are evaluated using different types of validation data. Additionally, Section 5 also includes a comparison of spatial patterns of LST and number of clear-sky days between the two products is presented. Finally, in Section 6 discussion and conclusions derived from the results are presented.

2. Data and study area

The objective of this work was to generate a refined LST product over the Amazon basin by re-processing MODIS level 1 data (at-sensor brightness temperatures) using a LST algorithm adapted to the surface and atmospheric conditions of the study area. We incorporated to the processing an external cloud mask, and daily LST values were also monthly averaged to produce both a daily and monthly LST product. Different products were used in the generation of the LST product discussed in this paper, as well as for intercomparison and validation analysis. A detailed description of each product is out of the scope of this paper, but we summarize in Table 1 the products used for this study, the purpose for which they were used, and a main reference for further details. The MODIS products were downloaded from ladsweb.nascom.nasa.gov, and MAIAC products used downloaded from dataportal.nccs.nasa.gov. The MAIAC cloud mask was also resized to 0.05° resolution from the reprojected product at 0.009°. In this case, clear sky days were selected as having only one pixel being cloudy within the resampling window.

All the products were subset to a region defined by [10N–20S, 80W–45W] geographical lat/lon (datum WGS84). Because we are only interested on the Amazon tropical forest, a vegetation mask was constructed as the intersection of pixels classified as “Evergreen Broadleaf Forest-EBF” in MCD12Q1 and MCD12C1 land cover products and a geographical vector covering the political regions of Amazonia (Fig. 1).

The ground in situ LST used in the validation analysis was derived from a permanent validation station situated at Tambopata (12.818S, 69.281W), in the Peruvian Amazon. This station is situated in a relatively homogeneous area characterized by dense tropical forest making it less problematic to deal with the upscaling issue of data points to pixel size data (Fig. 1). Two different thermal radiometers T_SI111 and IR_120 are installed above the canopy, providing average radiometric temperature values every 5 min from December 2014 to present. The time period of data recording considered in this paper is from December of 2014 since October of 2016. A similar in in situ configuration and in situ data processing can be found in Mattar et al. (2016).

3. LST algorithm

LST retrieval of current MOD11A1/MYD11A1 LST products uses a Split-Window (SW) algorithm (Wan and Dozier, 1996) in which the coefficients consider the dependence of view angle, total column water and surface air temperature through the use of multi-dimensional look-up tables. The MOD11C1/MYD11C1 product is based on the day/night algorithm (Wan and Li, 2008) which retrieves surface spectral emissivity and temperature from a pair of daytime and night-time MODIS data in TIR bands 20, 22, 23, 29 and 31–32.

In this study in order to test an alternative LST retrieval algorithm we suggest the use of the theoretical Split-Window model developed by Sobrino et al. (1996) for the retrieval of the daytime vegetation LST. Two assumptions are considered in order to derive the mathematical structure presented here: 1) dependence on emissivity terms results in a constant value which can be integrated in the c_0 term (tropical forests with dense green vegetation are well represented by typical vegetation emissivity), and 2) dependence on water vapour is considered implicitly in the derivation of c_1 and c_2 terms, thus eliminating the need of introducing water vapour information in the algorithm. Doing this, the mathematical structure results in:

$$T_s = T_i + c_0 + c_1(T_i - T_j) + c_2(T_i - T_j)^2 \quad (1)$$

where T_i and T_j represent the brightness temperatures of bands 31 and 32 of MODIS sensor, respectively, and c_i are the algorithm coefficients obtained from simulated data (Table 2).

This algorithm benefits from a minimum input data requirement, only the brightness temperatures of bands 31 and 32, in comparison to current MODIS LST retrieval algorithm (MOD11) in which different auxiliary data or independent day/night observations are required. Additionally, the mathematical structure presented here was tested against Wan and Dozier (1996) structure considering the same two assumptions described previously. Validation with in-situ data showed a difference in RMSE (SW algorithm minus Wan and Dozier expressed in mean ± standard deviation, with units of K) of -0.100 ± 0.017/ -0.75 ± 0.06, 0.15 ± 0.30/ -0.85 ± 0.14 for the different MODIS cases (MOD/MYDA1, MOD/MYDC1) (analysis shown in the supplementary material).

Algorithm coefficients were derived by statistical linear regression of a simulated dataset of brightness temperatures (T_i, T_j) over different surface and atmospheric conditions. This database was generated from forward simulations driven by the Radiative Transfer Equation (RTE), emissivity spectra, and input atmospheric profiles to the MODTRAN (v5.20) radiative transfer code (Berk et al., 2008). All the spectral magnitudes were convolved to the spectral response functions of MODIS bands. Three vegetation spectra (grass, coniferous and deciduous) were selected from the ASTER spectral library (Baldridge et al., 2009), whereas atmospheric profiles were extracted from the MODIS atmospheric profile product (MOD07 and MYD07, version 6).

MOD07/MYD07 cloud-free profiles were collected from 1118 spatial reference points within the study area for the 2014–2016 time period. In order to reduce the possible cloud contamination effect in

Table 1
MODIS products used in the generation of the LST product and data analysis.

Modis product	Layer	Version	Spatial resolution	Reference	Purpose
MOD07_L2/MYD07_L2	Retrieved temperature profile Retrieved dew point temperature profile Retrieved geopotential height profile	6	Swath	Seemann et al. (2006)	LST product generation
MODTBGA/MYDTBGA	Band 31, band 32	6	1 km sinusoidal	Boschetti and Vermote (2015)	LST product generation
MOD09CMG/MYD09CMG	Band 31, band 32	6	5 km geographic lat/long	Vermote (2015)	LST product generation
MAIACTBRF/MAIACATBRF	Status_QA	6	1 km sinusoidal	Lyapustin et al. (2008)	LST product generation
MOD11A1/MYD11A1	LST_Day_1km/QC_Day	5	1 km sinusoidal	Wan and Dozier (1996)	Product comparison
	Day_view_time	6			
MOD11C1/MYD11C1	LST_Day_CMG	5	5 km geographic lat/long	Wan and Li (1997)	Product comparison
	QC_Day	6			
	Day_view_time				
MCD12Q1	Land Cover Type 1 (IGBP)	5.1	1 km sinusoidal	Strahler et al. (1999)	Vegetation mask generation
MCD12C1	Land Cover Type 1 (IGBP)	5.1	5 km geographic lat/long	Strahler et al. (1999)	Vegetation mask generation

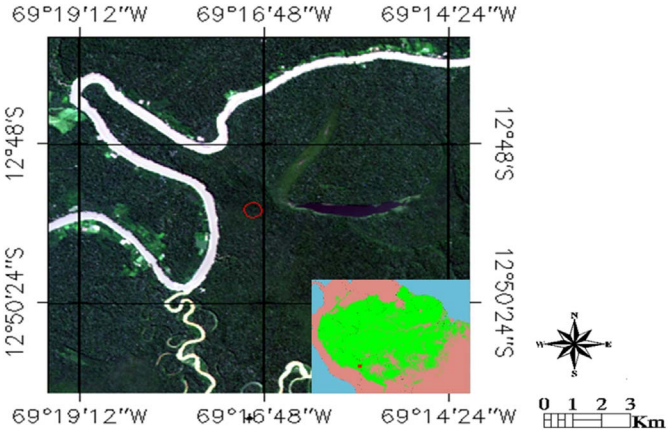

Fig. 1. Location of the Tambopata validation site in the Peruvian Amazon (view extracted from a colour composition using Landsat-8). In the lower right corner the mask for the evergreen broadleaf forests is coloured in green. (For interpretation of the references to colour in this figure legend, the reader is referred to the web version of this article.)

Table 2
Split-Window algorithm coefficients (Eq. (1)) for MODIS/TERRA and MODIS/AQUA data together with the standard error of estimation of the algorithm (δ_{alg}) derived in the coefficient retrieval process.

	c_1	c_2 (K^{-1})	c_0 (K)	δ_{alg} (K)
TERRA	2.208	0.629	1.461	0.48
AQUA	1.638	0.774	1.829	0.62

atmospheric profiles values the average radiance of the pixels considered clear in a 5 × 5 field of view area of the MOD07/MYD07 product was considered as representative of the spatial points. The total amount of simulated data points for the MODIS/TERRA case was 542,000 and for the MODIS/AQUA case 870,000. These two datasets were splitted into a train dataset (70%) and a test dataset (30%). The SW coefficients derived from the training dataset are included in Table 2.

The performance of the algorithm was initially assessed using the test dataset. Fig. 2 (left column) shows the difference between the temperature extracted from the first layer of the atmospheric profile (T_{MOD07}) and the temperature calculated with the SW algorithm (T_{alg}) versus the water vapour content observed along the satellite viewing path for both TERRA and AQUA platforms. The temperature difference ranges from −1 K to 3 K for water vapour values ranging from approximately 1 g/cm^2 to 12 g/cm^2. Differences are within ± 1 K for water vapour values lower than 8 g/cm^2, with frequent values for this region lying in the interval 1–7 g/cm^2. Differences increase up to 2 K for extremely high water vapour contents (> 8 g/cm^2).

Fig. 2 (middle column) also shows the difference T_{MOD07}-T_{alg} versus the satellite View Zenith Angle (VZA). In this case, for both TERRA and AQUA and considering the box (quartile 1 to quartile 4) there is a positive increase of this difference for higher values of VZA. This becomes especially evident from the box at 40°–50°. In both cases, temperatures differences are around 4 K. However, in spite the presence of possible outliers, we can observe that the boxes lie within the range of ± 1 K.

Basis statistics for the performance of the SW algorithm are graphically presented in Fig. 2 (right column). A null bias is obtained for both MODIS/TERRA and MODIS/AQUA cases, with 1-sigma standard deviations of 0.5 K and 0.6 K, respectively. These results are in accordance with the standard error of estimation of the algorithm using the training dataset (see Table 2).

4. Cloud masks: MOD35 vs MAIAC

Identifying cloud interference in satellite-derived data is a critical step in the development of remote sensing products (Wilson et al., 2014). In particular for the LST products generation temperature alterations (a systematic bias toward colder-than-true values) could be introduced if the cloud-contamination is not properly addressed (Østby et al., 2014; Williamson et al., 2013; Westermann et al., 2012). Thus a proper cloud mask is needed in order to fully consider this effect.

Current retrieval of MODIS LST products (MOD11) is based in the MOD35 cloud masking methodology (Ackerman et al., 2010). Depending on the surface type and solar illumination, this approach uses a combination of a variety of spectral threshold tests in order to provide the level of confidence of a pixel being clear. This level is assessed using four different categories: confident clear (> 99%), probably clear (> 95%), uncertain/probably cloudy (> 66%) and cloudy (< 66%).

MAIAC cloud mask (Lyapustin et al., 2008) is a time-based approach in which clouds are detected using a combination of spectral and brightness tests together with some pre-build reference clear images. Covariance analysis is used in order to build these reference images. This algorithm also possesses a dynamic land-water-snow mask, which guides the surface and aerosol retrieval in rapid changing conditions, such as fires and floods. The outputs provided by this cloud detection are CM_CLEAR, CM_CLOUD, and CM_PCLOUD corresponding to clear, cloudy and possibly cloudy.

In Fig. 3 a statistical comparison of these two approaches for the year 2014 is showed. MOD35 cloud mask flags were extracted from the QC layer in the MOD11A1V6 product ("LST not produced due to clouds" corresponding to 'probably cloudy' + 'cloudy' categories), whereas MAIAC cloud flags were extracted from the STATUS QC layer of the MAIACTBRF product ('cloudy' + 'possible cloudy'). An additional cloud flag (QC) was considered based on the retrieval quality embedded in the QC layer ("LST not produced due to clouds" + "LST other quality") (Nishida et al., 2003; Williamson et al., 2013). The

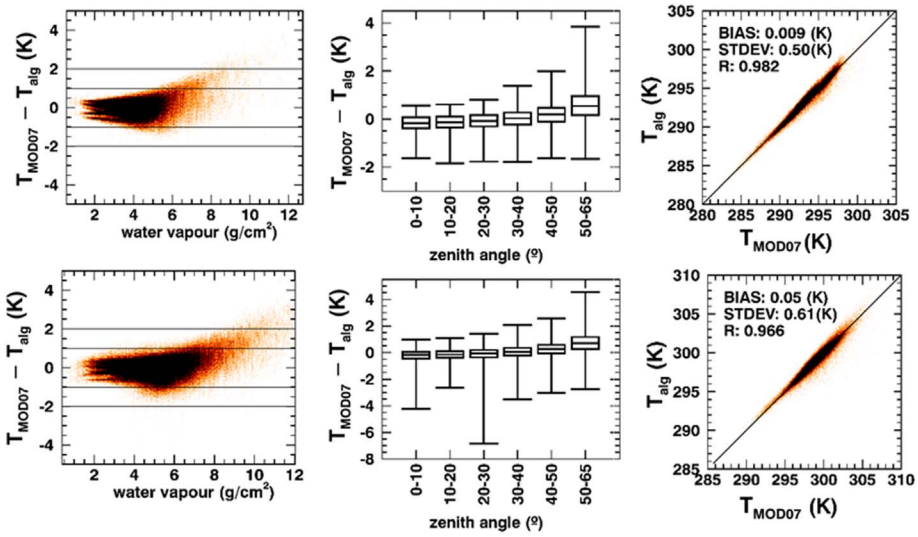

Fig. 2. Testing of the SW algorithm using the simulated data included in the test dataset for the MODIS/TERRA (first row) and MODIS/AQUA (second row) cases. Differences between the temperature extracted from the atmospheric profile (T_{MOD07}) and the temperature estimated with the SW algorithm (T_{alg}) are represented versus the atmospheric water vapour (left column) and the satellite view zenith angle (middle column). Basic statistics for the performance of the algorithm are included in the right column. In the graphs presented in the left and right columns, the density of points for a particular interval is linked to the intensity of the colour.

metrics used for comparison are: difference in the number of total cloudy days, Probability of Detection (POD) for both the cloudy and clear classes and False Alarm Ratio (FAR) for both the cloudy and clear classes (Karlsson and Dybbroe, 2010). In Table 3 the contingency matrix together with comparison scores is presented. For cloud masks that are similar POD values should be close to 1 and FAR values are minimized. For the comparisons MAIAC is considered as the ground truth data.

As we can see from the difference in number of cloudy days in Fig. 3, MAIAC flags more pixels as clouds than MOD35 for both sensors TERRA and AQUA. It is especially evident in the north-eastern region. In comparison against QC we see that for TERRA MAIAC flags a similar amount of clouds as QC (± 10), with a positive difference in the eastern and western predominantly and a negative difference in the centre of the region. For AQUA platform, MAIAC flags less clouds than QC for the entire region. Taking into account the POD and FAR we see that for TERRA and AQUA the same behaviour is reproduced. For the analysis we have that due to the continuous cloud coverage over the region the cloudy class is more predominant than the cloud-free class (i.e. d > a, b, c). For the comparison MAIAC-MODIS we see that POD cloudy have values closer but not equal to 1 thus implying the existence of a c value which is more important for AQUA than TERRA (MAIAC considers cloudy what MOD35 considers clear). FAR however is almost 0 for both cases. As MAIAC is more restrictive than MOD35 the majority

Table 3
Contingency matrix for the different cloud masks used for comparison together with validation scores. MAIAC is considered as ground reference.

	MODIS (QC) cloud free	MODIS (QC) cloudy	POD
MAIAC cloud free	a	b	a / (a + b) (cloud-free)
MAIAC cloudy	c	d	d / (c + d) (cloudy)
FAR	c / (a + c) (cloud-free)	b / (b + d) (cloudy)	

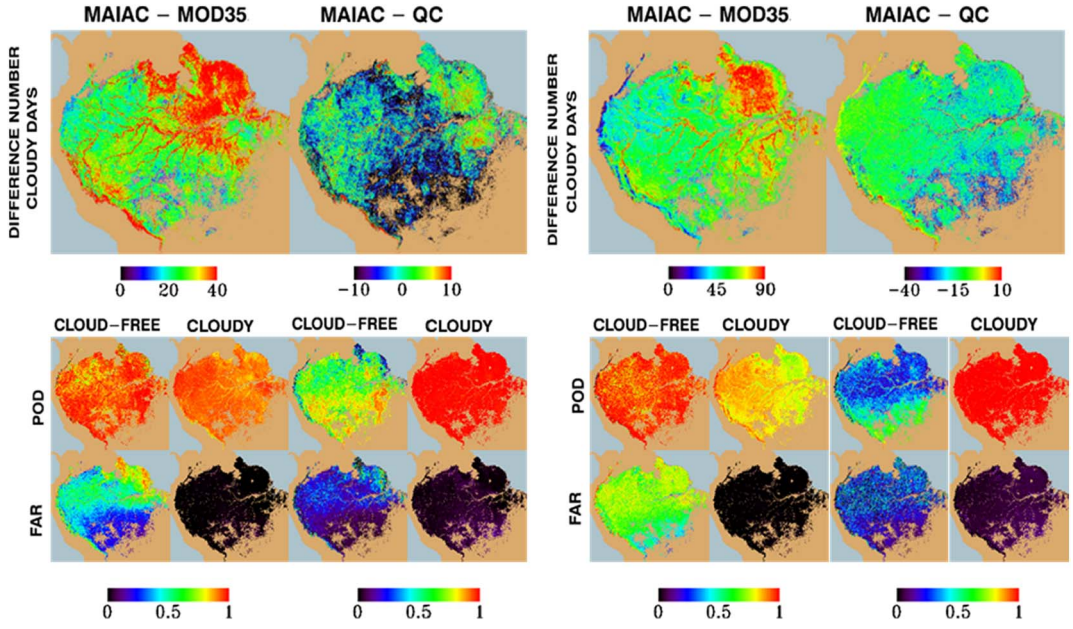

Fig. 3. Statistical comparison of the cloud masks considered in the study for TERRA platform (left) and AQUA platform (right) for the year 2014. For each platform first column and second column represents MAIAC-MODIS and MAIAC-QC results respectively. First row is the difference in the number of cloudy days, second and third row are the POD, probability of detection (cloud-free and cloudy) and FAR, False Alarm Ratio (cloud-free, cloudy) respectively.

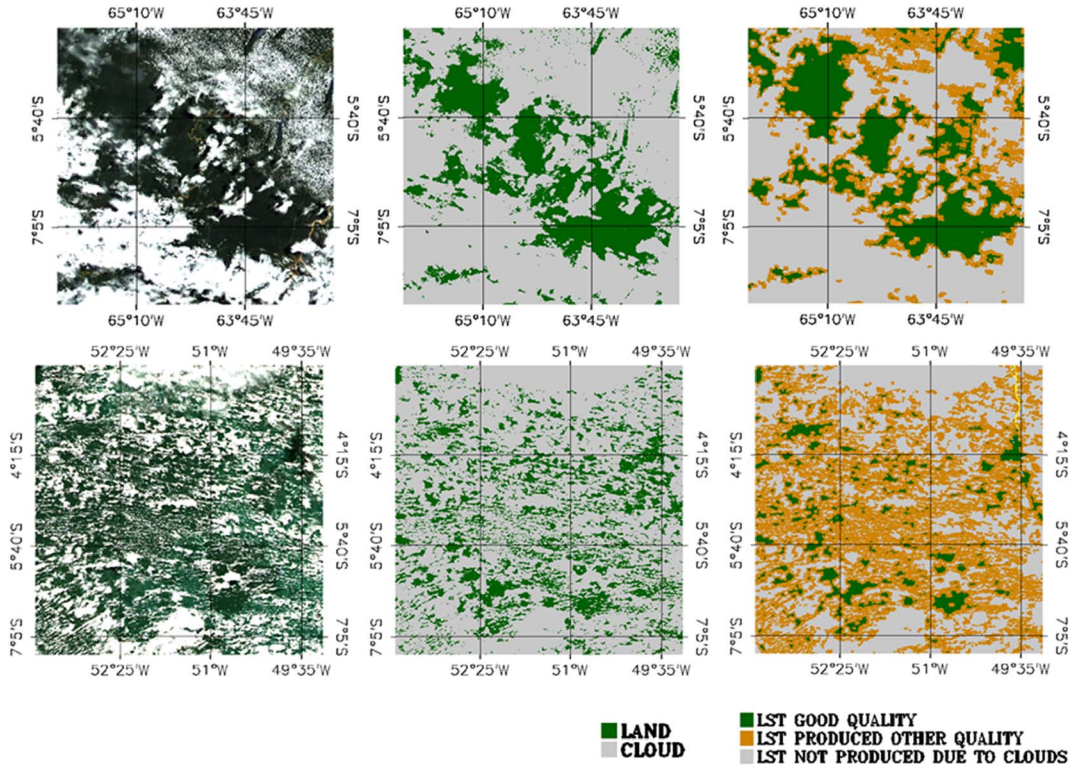

Fig. 4. Visual comparison of the clouds mask considered in the study for two different regions within the study area. Top row is DOY 198 for TERRA sensor. Bottom row is DOY 147 for AQUA sensor. First column is a true colour view of the region, middle column MAIAC cloud mask and third column is MOD35/QC cloud mask.

of MOD35 cloud pixels are also MAIAC cloud pixels (d big and b small). MAIAC-MODIS cloud-free has also POD values closer to one but in this case FAR values are higher than for the cloudy class. MAIAC-QC POD and FAR cloudy class for both TERRA and AQUA have values closer to one and 0 respectively. However FAR values have increased in comparison of MAIAC-MODIS cloudy (i.e. b has bigger values and c has lower values than the previous case). This is also evident for the cloud-free class with FAR minimized and POD minimized. For QC MAIAC, QC masks as cloud what MAIAC flags as clear.

In Fig. 4 a visual comparison for TERRA (upper row) and AQUA (lower row) of the cloud masks is showed. They correspond to Day of the Year (DOY) 198 and 147 respectively. As we see MAIAC provides a better representation of the cloud-class in comparison with MOD35 and QC. MOD35 flags less pixels as clouds than MAIAC. QC in contrast tends to flag more pixels as clouds for AQUA (clouds are more distributed) than for TERRA. The major point of MAIAC is that it able to better capture the thin or small clouds in comparison to MOD35 cloud mask (Lyapustin et al., 2008). This is especially important for regions where small clouds tend to prevail, such as the northeast of the study region and additionally at AQUA overpass time when clouds are more distributed.

5. Validation results

5.1. In situ data

Radiometric temperatures (T_r) measured in situ were converted to LST (T_s) after correction of down-welling atmospheric sky irradiance (L^{down}) and surface emissivity (ε):

$$B_i(T_s) = \frac{B_i(T_r) - (1 - \varepsilon_i)L_i^{down}}{\varepsilon_i} \quad (2)$$

The L_i^{down} term was derived by using MODTRAN code and the atmospheric profiles extracted from the MOD07 and MYD07 products. In the case of missing values in the MOD/MY07 products a seasonal mean value was applied. We assumed an emissivity value of 0.99 for the green and dense vegetation canopy. LST values derived from the two radiometers were averaged for the validation analysis.

LSTs derived from in situ data were compared against MODIS LSTs extracted for the pixel located at the test site using both standard products (MOD11) and the SW-based product. Such a comparison was performed at three different levels of cloud masking: i) the MOD35 cloud mask as included in the MOD11 product without any additional QA discrimination (LST not produced due to clouds), ii) the MOD35 cloud mask as included in the MOD11 product and the additional filter based on the QC layer (LST not produced due to clouds + LST produced other quality) (Nishida et al., 2003; Williamson et al., 2013), and iii) the MAIAC cloud mask. For simplicity, we will refer to these three cases as MOD35, QC and MAIAC, respectively. Validation results are presented in Fig. 5 for the three cases (MOD35, QC, MAIAC) and also for different MODIS (Terra & Aqua) standard LST products (MOD/MYDA1, MOD/MYDC1). Results presented in Fig. 5 are complemented with basic error metrics (bias, standard deviation and Root Mean Square Error) included in Fig. 6. Error metrics were derived considering ($T_s - T_{alg}$). Tabulated values of these metrics are also provided in the supplementary material.

Starting with the MOD11A1 case we see in terms of RMSE the SW algorithm gives better results than daytime MOD11A1 product for all the cloud mask stages considered having a difference (MODIS minus SW) of 0.63 K (MOD35), 1.08 K (QC), and 0.98 K (MAIAC). This is mainly due to the reduction of the bias (values closer to the 1:1 line, Fig. 5), whereas the standard deviation for the SW is similar to that of the MODIS LST standard product (MOD11A1). In the case of MOD35 SW we see however an increase in the value due to the cloud contamination effect. It also must be worth noting that SW MAIAC case provides better results than MODIS QC and MODIS MOD35, having differences of RMSE values of around 1 and 2 K, respectively.

For the case of MYD11A1 the same behaviour is reproduced. There is a difference in RMSE between MODIS LST (MYD11A1) and SW of approximately 0.7 and 0.6 K for the QC and MAIAC case. For the

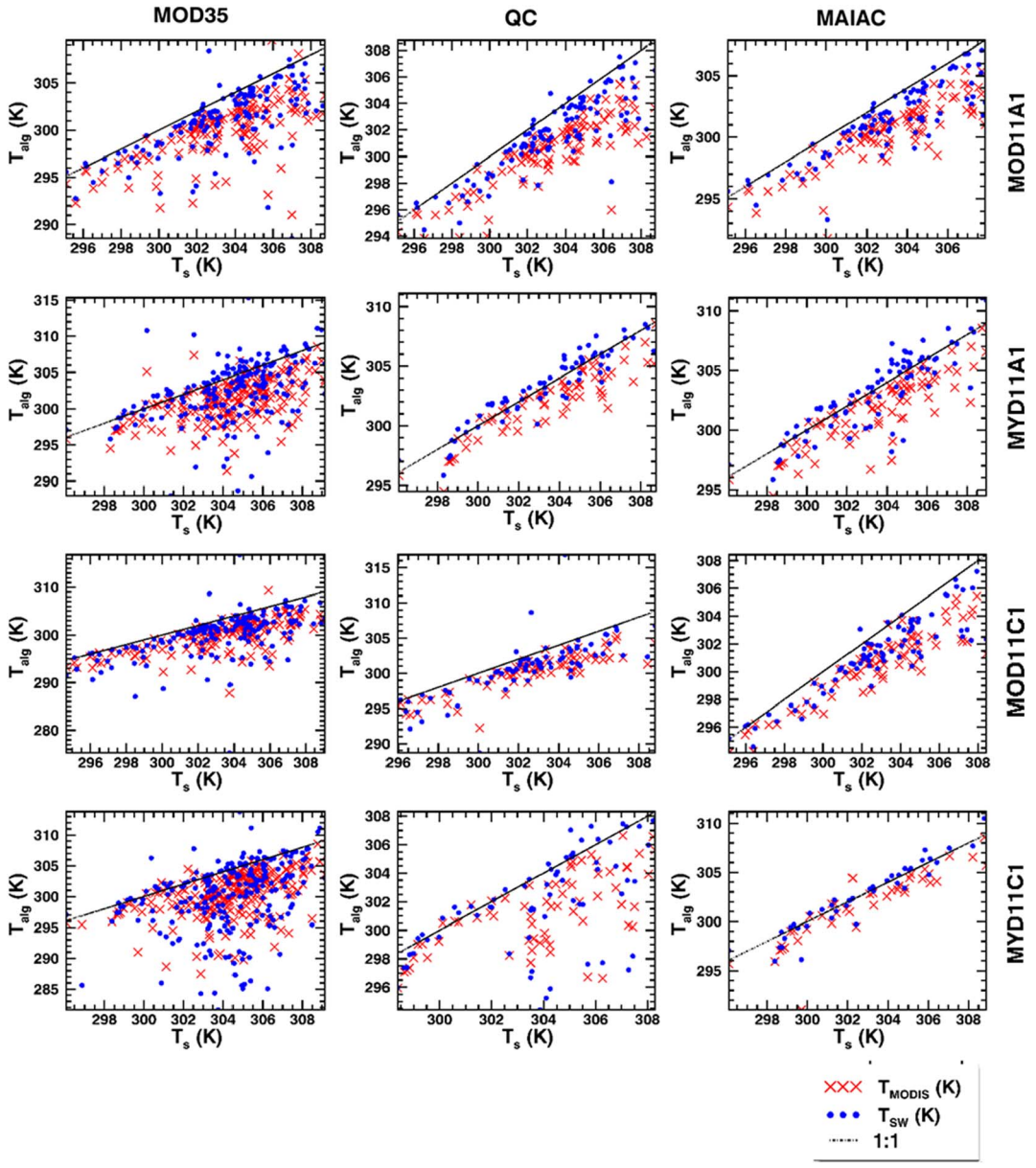

Fig. 5. Ground measured T_s against T_{MODIS} (red cross) and T_{SW} (blue filled circle) for the three cloud mask stages of comparison: left column (LST not produced due to clouds), middle column (LST good quality), right column (MAIAC cloud mask) and for the LST products considered: MOD11A1 (first row), MYD11A1 (second row), MOD11C1 (third row) and MYD11C1 (fourth row). The line 1:1 is also represented. (For interpretation of the references to colour in this figure legend, the reader is referred to the web version of this article.)

MOD35 both SW and MODIS provide similar values. This results from a reduction in the bias. For the case of the standard deviation we see that due to the filtering of possible clouds there is a reduction of the standard deviation for the QC and MAIAC cases for both MODIS and SW. In the MOD35 case there is a difference in standard deviation of approximately 1.1 K. As in the MOD11A1 case, this is due to the cloud contamination effect. The SW is much affected by the presence of possible clouds requiring of an accurate cloud masking in order to provide accurate results. Additionally, MAIAC is able to provide more cloud-free pixels than QC. Finally the SW MAIAC provides a reduction in the RMSE of 0.2 K and 2.4 K when compared to MODIS QC and MODIS MOD35, respectively.

For the case of C1 products MODIS MOD35 and MODIS QC cases provides better results than SW. Due to the lower spatial resolution these products are probably more cloud contaminated. This results in higher values of RMSE. However we see that when applying MAIAC cloud mask the behaviour is inverted. SW provides a lower value of bias and similar value of standard deviation regarding than MOD35, thus providing lower values of RMSE. For the MOD11C1 product, SW MAIAC provides a reduction of approximately 0.8 K and 2.2 K when compared to QC MODIS and MOD35 MODIS. Additionally SW MAIAC is able to provide more cloud-free pixels. For the MYD11C1 product the reduction in the RMSE is approximately 2.4 K and 4 K when compared to QC MODIS and MOD35 MODIS.

Eventually, the comparison was also carried out on MODIS version 5 LST products (results included in the supplementary material). Conclusions are similar to those extracted from the v6 comparisons, but RMSE values are higher for the v5.

5.2. R-based method

The validation analysis was extended to a set of around 100 additional pixels randomly selected within the study area. This additional analysis was performed using the so called R-based validation method, which does not require in situ data (Wan and Li, 2008; Coll et al., 2012). The R-based method is physically based on the inversion of the

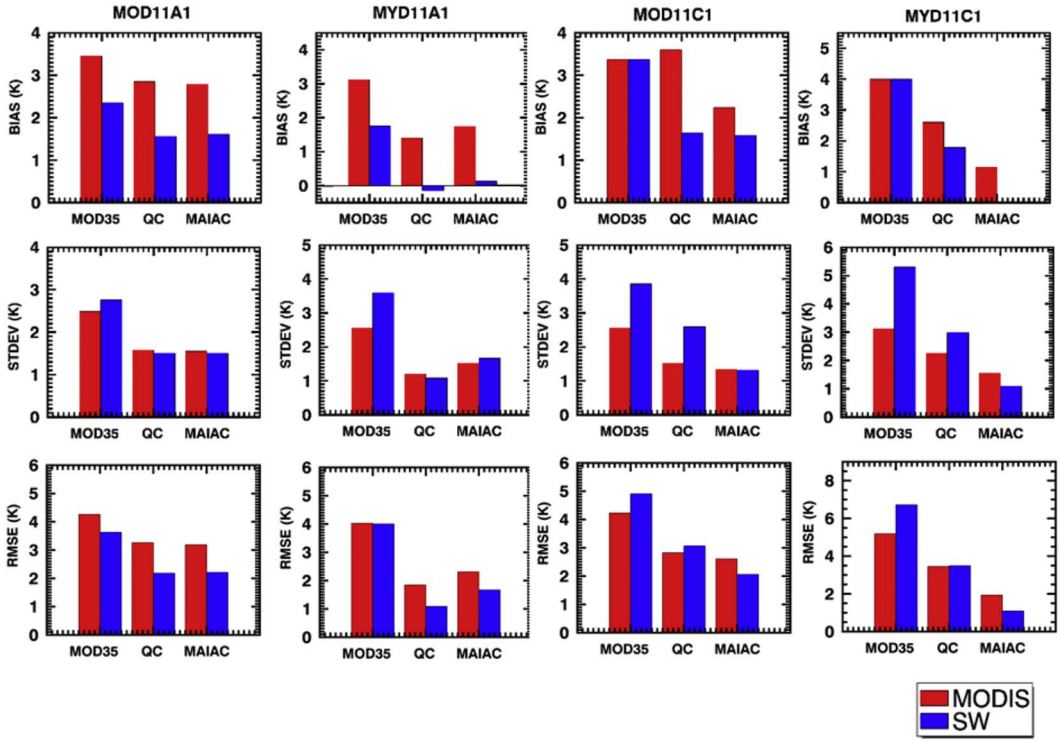

Fig. 6. Error metrics for the three stages of comparison, LST not produced due to clouds (MOD35), LST having good quality (QC) and MAIAC cloud mask (MAIAC) considering the LST values derived from the MODIS LST products (MOD11) (red) and split-window algorithm (blue). Error metrics were calculated considering the difference $T_s - T_{alg}$. (For interpretation of the references to colour in this figure legend, the reader is referred to the web version of this article.)

radiative transfer equation to obtain the reference LST (LST_R). The inversion is performed for each pixel using MOD/MYD07 atmospheric profiles and a constant value of 0.99 for surface emissivity. LST_R was retrieved from MODIS band 31, and a quality control was applied to the LST retrievals based on the difference between the observed brightness temperature at band 32 and the simulated brightness temperature at that band (ΔT_{b32}), as suggested by Wan and Li (2008).

The optimal threshold value for ΔT_{b32} is selected so that the difference between the simulated LST_R and the actual LST lies within ± 1 K. For this purpose, the pixel centred at the Tambopata test site was selected, where in situ LSTs are available (Section 5.1). According to the results presented in Fig. 7, the threshold values $-0.1\,K < \Delta T_{b32} < 0.3\,K$ provides a difference of ± 1 K in the difference between the R-based temperature and the LST in situ. However, taking into account the limitations in the number of clear-sky pixels imposed by the study region a final threshold of $-0.2\,K < \Delta T_{b32} < 0.4\,K$ was considered in order to increase the number of points. This recalculated threshold values provide a difference of less than ± 2 K (Fig. 7; Table 4), which is in agreement with research communities requirements (GCOS, 2006).

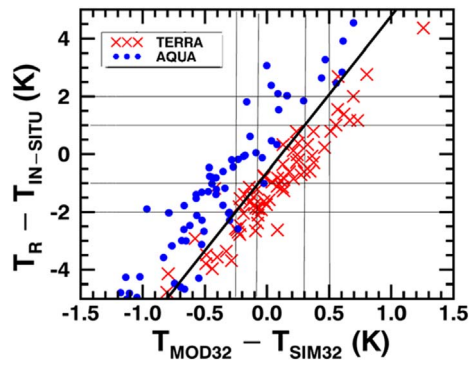

Fig. 7. Determination of the optimal threshold value for ΔT_{b32} ($T_{MOD32} - T_{SIM32}$). ΔT_{b32} is represented against the difference between the T_R (derived from the R-based method) and $T_{IN\text{-}SITU}$ as derived in the Section 5.1.

Table 4
Error metrics derived from the comparison of in situ LST against reference LST obtained with the R-based method over the Tambopata test site considering a threshold of $-0.2\,K < \Delta T_{b32} < 0.4\,K$. RMSE: Root Mean Square Error, MAE: Mean Absolute Error, N: number of data points.

	Bias	sdtev	RMSE	MAE	N
MODA1	1.08	1.16	1.58	1.20	44
MYDA1	− 0.99	1.18	1.54	1.17	15
MODC1	1.37	1.23	1.85	1.43	38
MYDC1	− 0.73	1.30	1.49	1.11	9

This threshold was applied to the test cases over the 100 pixels, and results are presented in Fig. 8. The proposed LST product shows lower values of bias and standard deviation in comparison with the current MODIS LST product (MOD11). The difference in terms of RMSE (MODIS − SW) is approximately of 0.9 K, 1.7 K, 0.7 K and 1.5 K for the MOD11A1, MYD11A1, MOD11C1 and MYD11C1 cases, respectively. Besides in spite the reduction of the initial spatial reference points considered the number of values is still elevated in order to provide a reliable validation dataset.

5.3. Analysis of spatial patterns

The validation analysis was completed with a comparison between the spatial patterns of clear-sky days and LST obtained from MODIS standard products and the LST product developed in this study. In particular, seasonal mean LST values together with the number of clear sky days per season for the year 2014 were used for comparison. Results from MOD11A1 and MYD11A1 cases were considered. Seasons included in the analysis were JFM (January–February–March), AMJ (April–May–June), JAS (July–August–September) and OND

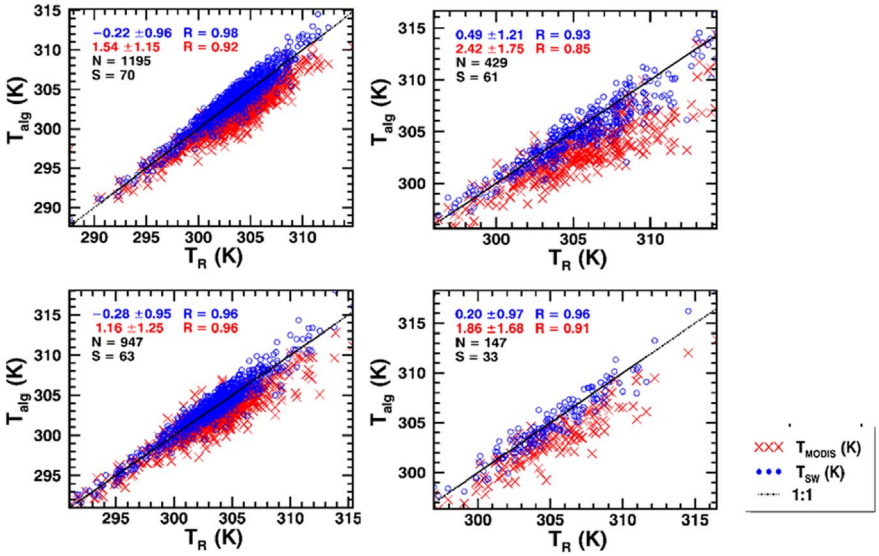

Fig. 8. Simulated R-based T_R against T_{MODIS} (red cross) and T_{SW} (blue circle) for the LST products considered: MOD11A1 (first row, first column), MYD11A1 (first row, second column), MOD11C1 (second row, first column) and MYD11C1 (second row, second column). Results include mean ± bias, correlation coefficient, N: total number of points and S: number of spatial points with data. The line 1:1 is also represented. (For interpretation of the references to colour in this figure legend, the reader is referred to the web version of this article.)

(October–November–December). Comparison was performed at the same three different levels of cloud masking than Section 5.1 (MOD35, QC and MAIAC). Additionally, spatial pattern validation was extended repeating this same procedure using Visible Infrared Imaging Radiometers Suite (VIIRS) data. Having satellite overpass time similar to AQUA and considered to be the successor of MODIS, VIIRS is presented as an add-on in order to validate the results derived from the LST presented here.

Considering MODIS results, the difference revealed in LST patterns between MOD35 and QC/MAIAC arise from the correction of cloud-contamination effect. QC and MAIAC spatial patterns are enhanced after removing the alteration (colder-than-true) of temperature introduced by clouds. The use of an additional cloud filtering however considerably reduces the number of available clear-sky-days (Fig. 9). This becomes especially evident for the northeast region for TERRA JFM/AJM, and AQUA QC JFM where after screening clouds it is produced a lack of available data. MOD35 provides more cloud-free pixels than QC/MAIAC (Fig. 9 and Fig. 3). MAIAC however it is able to provide more cloud-free pixels than QC for AQUA (Fig. 9 and Fig. 3) and also for TERRA (southeast region of AJM/JAS). These results agree well with previous studies (Hilker et al., 2012) in which MAIAC was shown to provide about 20–80% more cloud-free pixels depending on season than MYD09 surface reflectance product.

For the comparison of QC and MAIAC we see that MAIAC reproduces QC patterns. In this case, however the discrepancies due from an enhancement of some region by the LST product presented here cannot be properly addressed due to the low number of available points. However when comparing TERRA (equatorial crossing time 10:30 am) and AQUA (equatorial crossing time 1:30 pm) results we see that MAIAC spatial patterns agree well. A spatial warming located in the northern region predominantly during JFM/AJM and a more widespread warming for JAS and OND is observed for both TERRA and AQUA.

In Fig. 10 seasonally LST and number of clear-sky days is presented for VIIRS. In order to retrieve the LST an SW algorithm, using the same mathematical structure presented in this paper, was developed. The coefficients are presented in Table 5. They were derived using only AQUA simulated database for the year 2014. Brightness temperature of bands 15 and 16 were derived from the swath product NPP_VMAES_L1 (ladsweb.nascom.nasa.gov). Additionally, VNP35_L2 was considered for cloud masking. Obtained by heritage of MOD35_L2 product (MOD35 cloud mask) only pixels consider as confident clear were used for the LST retrieval.

Considering VIIRS and MAIAC AQUA results having both an equatorial crossing time of 1:30 pm we see that VIIRS reproduces AQUA spatial patterns. Additionally, VIIRS number of clear-sky days' spatial pattern is similar to MOD35.

6. Discussion and conclusions

The use of MODIS thermal satellite imagery has been proven as a valuable tool to monitor tropical forests (Jiménez-Muñoz et al., 2013, 2015b) being able to provide and independent measure of biophysical stress (Toomey et al., 2011). However, the use of surface temperature products still faces important limitations, mainly the cloud contamination effect aroused from an imperfect cloud masking. Additionally, the validation of their performance is problematic due to the restrictions imposed by the availability of in situ data.

In this work a comparative analysis between a MODIS daytime LST product resulting from the combination of updated split-window coefficients and the introduction of MAIAC cloud mask, and current MODIS LST products (MOD/MYD11A1, MOD/MYD11C1, version 6) was presented. The performance of both products was evaluated using temperature-based (in situ temperatures) and radiance-based validation methodologies. MODIS LST products (MOD11) were found to be severely cloud contaminated when additional QC is not considered, with overall RMSEs around 4–5 K. The deficient cloud detection is partly solved when using two alternative cloud filtering approaches: the QC layer and the MAIAC cloud mask. Additionally, the QC filtering is found to not provide a cloud masking similar to MAIAC (Figs. 3 and 4). The main improvement of MAIAC cloud mask is its ability to better capture the low, thin or small (sub-pixel) clouds (Lyapustin et al., 2011, 2012). However, the accuracy is improved at expenses of the reduction in data amount, especially for MYD products because of the later overpass of the Aqua platform. In the case of A1 products (with the nominal resolution ~1 km) the application of the MAIAC cloud mask leaded to a reduction of around 35% for MOD11A1 and 58% for MYD11A1. This reduction increased in the case of C1 products (climate grid at 0.05°), around 50% for MOD11C1 and 83% for MYD11C1 (see supplementary material).

Validation against in situ measurements showed a decrease of the RMSE for MODIS LST products (MOD11) when additional QC filtering or MAIAC is considered, with RMSEs around 2–3 K. The combination of the LST product presented in this paper with the MAIAC cloud mask was able to improve the RMSE, with final values of around 1–2 K.

The cloud masking is especially important for the generation of monthly or seasonal means of LST, as usually considered in climate related studies. When cloud detection is relaxed more clear sky pixels

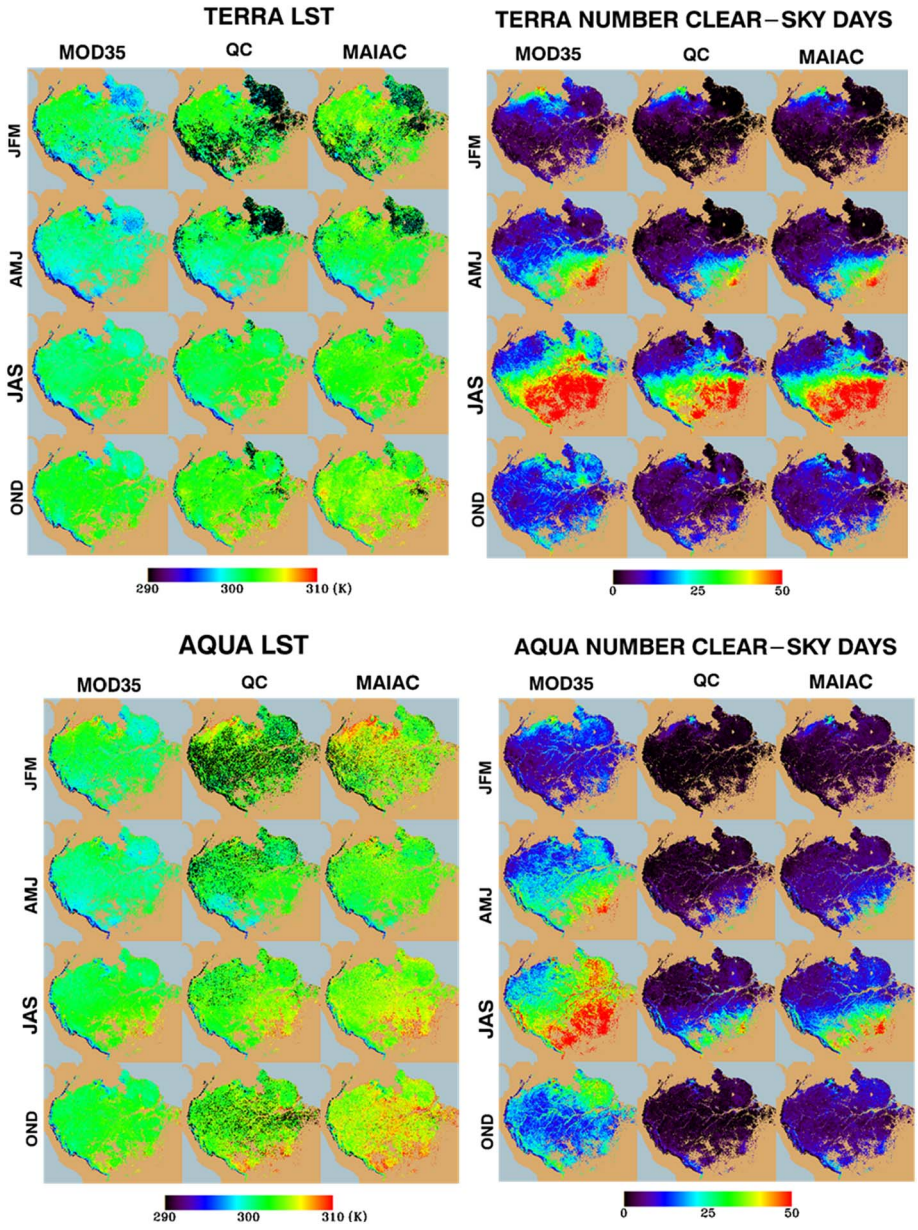

Fig. 9. Spatial patterns of LST (left image) and number of clear sky days (right image) for TERRA (upper part image) and AQUA (lower part image). For every panel the results are showed using rows as seasons (JFM, AMJ, JAS and OND.) and columns as cloud masks filtering (MOD35, QC and MAIAC).

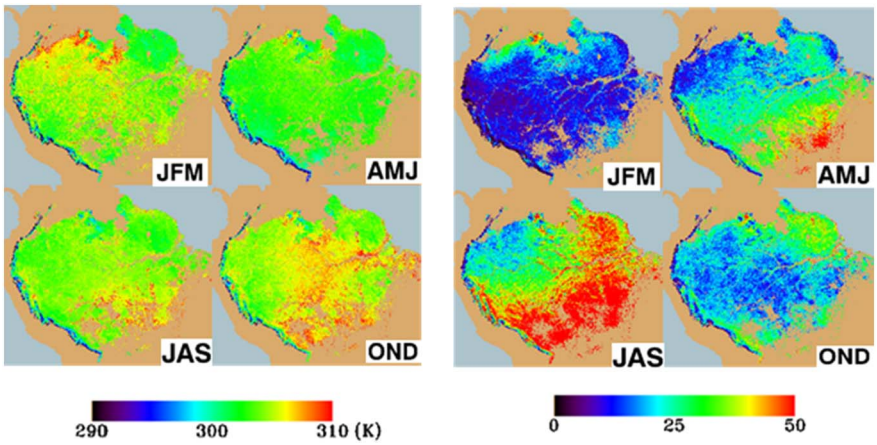

Fig. 10. Spatial patterns of LST (left image) and number of clear sky days (right image) for VIIRS sensor. Only confident clear pixels were considered for LST retrieval. For every panel the results are showed: JFM, AMJ, JAS and OND.

Table 5
Split-Window algorithm coefficients (Eq. (1)) for VIIRS data together with the standard error of estimation of the algorithm (δ_{alg}) derived in the coefficient retrieval process. Coefficients were obtained by using AQUA 2014 simulated database.

	c_1	c_2 (K^{-1})	c_0 (K)	δ_{alg} (K)
VIIRS	0.837	0.588	2.221	0.61

are available within a month, but the monthly mean may be biased because of the consideration of LST values for cloudy pixels in the computation of the mean value. In contrast, a very restrictive cloud detection leads to a decrease in the number of clear sky pixels, which jeopardizes the computation of a monthly mean over areas with high cloud cover occurrence. The MAIAC cloud mask provides a compromise with an accurate detection and an increase on the detection of clear sky pixels (Hilker et al., 2012). This is illustrated in the spatial patterns included in Fig. 9.

Detailed implications of deficient cloud masking and scarce number of clear sky days within a month over higher level products based on LST estimations (e.g. warming trends, drought monitoring) are still to be documented, although previous works referred in this paper demonstrated the usefulness of thermal data for these studies. We have also shown the potential of VIIRS LST products for the continuity of the MODIS LST series over the Amazon region. The LST products presented in this paper are available through the Thermal Amazoni@ interface (ipl.uv.es/thamazon/web) or under request to the authors.

In this study we provide evidence of the effect of heat stress which exacerbates aboveground biomass losses, indicating that models of tropical forest drought response should include both moisture and heat effects.

In this study we provide evidence of the effect of heat stress which exacerbates aboveground biomass losses, indicating that models of tropical forest drought response should include both moisture and heat effect.

Acknowledgements

This study was supported by Ministerio de Educación, Cultura y Deporte (grant FPU14/06502), Ministerio de Ciencia e Innovación (CEOS-Spain2, ESP2014-52955-R), and European Union and Ministerio de Economía y Competitividad (SIM project, PCIN-2015-232 ERA-LEARN 2020 WaterWorks-2014 cofunded call). The authors thank MODIS and MAIAC data teams for making data public available. Additionally we would like to thank Cristian Mattar (UChile), Andrés Santamaría-Artigas (UChile; University of Maryland), Eric Cosio (PUCP), and Fabián Limonchi (PUCP) for the technical assistance with the in situ data collected over the Tambopata test site. The *Servei de Càlcul* (University of Valencia) is also acknowledged for the services provided in the MODTRAN computations.

Appendix A. Supplementary data

Supplementary data to this article can be found online at https://doi.org/10.1016/j.rse.2017.10.015.

References

Ackerman, S., Strabala, K., Menzel, P., Frey, R., Moeller, C., Gumley, L., 2010. Discriminating clear-sky from cloud with MODIS algorithm theoretical basis document (MOD35). In: MODIS Cloud Mask Team. Cooperative Institute for Meteorological Satellite Studies, University of Wisconsin.

Baldridge, A.M., Hook, S.J., Grove, C.I., Rivera, G., 2009. The ASTER spectral library version 2.0. Remote Sens. Environ. 113, 711–715.

Berk, A., Anderson, G. P., Acharya, P. K., & Shettle, E. P. (2008). MODTRAN5. 2.0.0 User's Manual. Spectral Sciences Inc., Burlington, MA, Air Force Research Laboratory, Hanscom, MA.

Boschetti, L., Vermote, E., 2015. MODTBGA MODIS/Terra thermal bands daily L2G-Lite global 1 km SIN Grid V006. In: NASA EOSDIS Land Processes DAAC, http://dx.doi.org/10.5067/modis/modtbga.006.

Clark, D., Piper, S., Keeling, C., Clark, D., 2003. Tropical rain forest tree growth and atmospheric carbon dynamics linked to interannual temperature variation during 1984–2000. Proc. Natl. Acad. Sci. 100, 5852–5857.

Coll, C., Valor, E., Galve, J.M., Mira, M., Bisquert, M., García-Santos, V., et al., 2012. Long-term accuracy assessment of land surface temperatures derived from the Advanced Along-Track Scanning Radiometer. Remote Sens. Environ. 116, 211–225.

Dirzo, R., Raven, P.H., 2003. Global state of biodiversity and loss. Ann. Rev. Environ. Resour. 28, 137–167.

Doughty, C., Goulden, M., 2008. Are tropical forests near a high temperature threshold? J. Geophys. Res. Biogeosci. 113.

Galbraith, D., Levy, P., Sitch, S., Huntingford, C., Cox, P., Williams, M., Meir, P., 2010. Multiple mechanisms of Amazonian forest biomass losses in three dynamic global vegetation models under climate change. New Phytol. 187, 647–665.

GCOS, 2006. Systematic observation requirements for satellite-based products for climate-supplemental details to the satellite-based component of the implementation plan for the global observing system for climate in support of the UNFCCC. In: The Global Climate Observation System GCOS, pp. 107.

Gedney, N., Valdes, P., 2000. The effect of Amazonian deforestation on the northern hemisphere circulation and climate. Geophys. Res. Lett. 27, 3053–3056.

Gomis-Cebolla, J., Jiménez-Muñoz, J., Sobrino, J., 2016. MODIS-based monthly LST products over Amazonia under different cloud mask schemes. Data 1, 2.

Hilker, T., Lyapustin, A., Tucker, C., Sellers, P., Hall, F., Wang, Y., 2012. Remote sensing of tropical ecosystems: atmospheric correction and cloud masking matter. Remote Sens. Environ. 127, 370–384.

Hilker, T., Lyapustin, A., Hall, F., Myneni, R., Knyazikhin, Y., Wang, Y., Tucker, C., Sellers, P., 2015. On the measurability of change in Amazon vegetation from MODIS. Remote Sens. Environ. 166, 233–242.

Jiménez-Muñoz, J.C., Sobrino, J., Mattar, C., Malhi, Y., 2013. Spatial and temporal patterns of the recent warming of the Amazon forest. J. Geophys. Res. Atmos. 118, 5204–5215.

Jiménez-Muñoz, J.C., Mattar, C., Sobrino, J., Malhi, Y., 2015a. A database for the monitoring of thermal anomalies over the Amazon forest and adjacent intertropical oceans. Sci. Data 2, 150024.

Jiménez-Muñoz, J.C., Mattar, C., Sobrino, J., Malhi, Y., 2015b. Digital thermal monitoring of the Amazon forest: an intercomparison of satellite and reanalysis products. Int. J. Digital Earth 9, 477–498.

Jiménez-Muñoz, J.C., Mattar, C., Barichivich, J., Santamaría-Artigas, A., Takahashi, K., Malhi, Y., Sobrino, J.A., van der Schrier, G., 2016. Record-breaking warming and extreme drought in the Amazon rainforest during the course of El Niño 2015–2016. Sci Rep 6, 33130. http://dx.doi.org/10.1038/srep33130.

Karlsson, K.G., Dybbroe, A., 2010. Evaluation of Arctic cloud products from the EUMETSAT Climate Monitoring Satellite Application Facility based on CALIPSO-CALIOP observations. Atmos. Chem. Phys. 10 (4), 1789–1807.

Leinenkugel, P., Kuenzer, C., Dech, S., 2013. Comparison and enhancement of MODIS cloudmask products for Southeast Asia. Int. J. Remote Sens. 34 (8), 2730–2748. http://dx.doi.org/10.1080/01431161.2012.750037.

Lyapustin, A., Wang, Y., Frey, R., 2008. An automatic cloud mask algorithm based on time series of MODIS measurements. J. Geophys. Res.-Atmos. 113 (D16), D16207.

Lyapustin, A., Wang, Y., Laszlo, I., Kahn, R., Korkin, S., Remer, L., Levy, R., Reid, J.S., 2011. Multi-angle implementation of atmospheric correction (MAIAC): part 2. Aerosol algorithm. J. Geophys. Res. 116, D03211. http://dx.doi.org/10.1029/2010JD014986.

Lyapustin, A., Wang, Y., Laszlo, I., Korkin, S., 2012. Improved cloud screening in MAIAC aerosol retrievals using spectral and spatial analysis. Atmos. Meas. Tech. Discuss. 5, 1575–1595. http://dx.doi.org/10.5194/amtd-5-1575-2012.

Malhi, Y., Roberts, J., Betts, R., Killeen, T., Li, W., Nobre, C., 2008. Climate change, deforestation, and the fate of the Amazon. Science 319, 169–172.

Mattar, C., Santamaría-Artigues, A., Durán-Alarcón, C., Olivera-Guerra, L., Fuster, R., Borvarán, D., 2016. The LAB-net soil moisture network: application to thermal remote sensing and surface energy balance. Data 1, 6.

Nishida, K., Nemani, R.R., Glassy, J.M., Running, S.W., 2003. Development of an evapotranspiration index from Aqua/MODIS for monitoring surface moisture status. IEEE Trans. Geosci. Remote Sens. 41, 493–501.

Østby, T., Schuler, T., Westermann, S., 2014. Severe cloud contamination of MODIS land surface temperatures over an Arctic ice cap, Svalbard. Remote Sens. Environ. 142, 95–102.

Seemann, S.W., Borbas, E.E., Li, J., Menzel, W.P., Gumley, L.E., 2006. MODIS Atmospheric Profile Retrieval Algorithm Theoretical Basis Document. Version 6. pp. 25.

Sobrino, J.A., Li, Z.L., Stoll, M.P., Becker, F., 1996. Multi-channel and multi-angle algorithms for estimating sea and land surface temperature with ATSR data. Int. J. Remote Sens. 17 (11), 2089–2114.

Strahler, A., et al., 1999. MODIS land cover product. In: Algorithm Theoretical Basis Document Version 5.0. Boston University.

Toomey, M., Roberts, D., Still, C., Goulden, M., McFadden, J., 2011. Remotely sensed heat anomalies linked with Amazonian forest biomass declines. Geophys. Res. Lett. 38.

Vermote, E., 2015. MOD09CMG MODIS/Terra surface reflectance daily L3 global 0.05Deg CMG V006. In: NASA EOSDIS Land Processes DAAC, http://dx.doi.org/10.5067/modis/mod09cmg.006.

Wan, Z., Dozier, J., 1996. A generalized split-window algorithm for retrieving land-surface temperature from space. IEEE Trans. Geosci. Remote Sens. 34 (4), 892–905.

Wan, Z., Li, Z., 2008. Radiance-based validation of the V5 MODIS land-surface temperature product. Int. J. Remote Sens. 29, 5373–5395.

Werth, D., Avissar, R., 2002. The local and global effects of Amazon deforestation. J. Geophys. Res. Atmos. 107, 8087.
Westermann, S., Langer, M., Boike, J., 2012. Systematic bias of average winter-time land surface temperatures inferred from MODIS at a site on Svalbard, Norway. Remote Sens. Environ. 118, 162–167.
Williamson, S.N., Hilk, D.S., Garnon, J.A., Kavanaugh, J.L., Koh, S., 2013. Evaluating cloud contamination in clear-sky MODIS Terra daytime land surface temperatures using ground-based meteorology observations. J. Clim. 26 (5), 1551–1600.
Wilson, A., Parmentier, B., Jetz, W., 2014. Systematic land cover bias in Collection 5 MODIS cloud mask and derived products — a global overview. Remote Sens. Environ. 141, 149–154.